Electronic Supplementary Material (ESI) for Materials Chemistry Frontiers.
This journal is © the Partner Organisations 2022

Supporting Information

Synergetic Model for Implementing Single-Component White-Light Emission: A Case Study of Zero-Dimensional Cadmium Halides

Jiantao Yuan,[a] Guojun Zhou,[a] Jian Zhang,[a] Xian-Ming Zhang*[a,b]

[a] *Key Laboratory of Magnetic Molecules and Magnetic Information Materials (Ministry of Education), School of Chemistry and Material Science, Shanxi Normal University, Taiyuan 030006, China. Email: zhangxm@dns.sxnu.edu.cn*

[b] *College of Chemistry & Chemical Engineering, Key Laboratory of Interface Science and Engineering in Advanced Material, Ministry of Education, Taiyuan University of Technology, Taiyuan, Shanxi 030024, P. R. China*

Contents

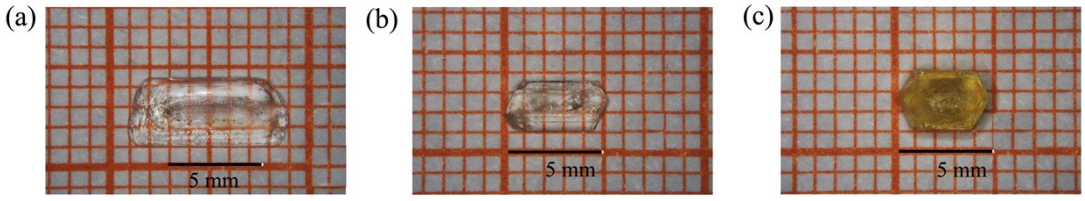

Figure S1. Photographs of $(C_6H_7NCl)_2CdCl_4$ (a), $(C_6H_7NBr)_2CdBr_4$ (b) and $(C_6H_7NI)_2CdI_4$ (c) crystals upon natural light.

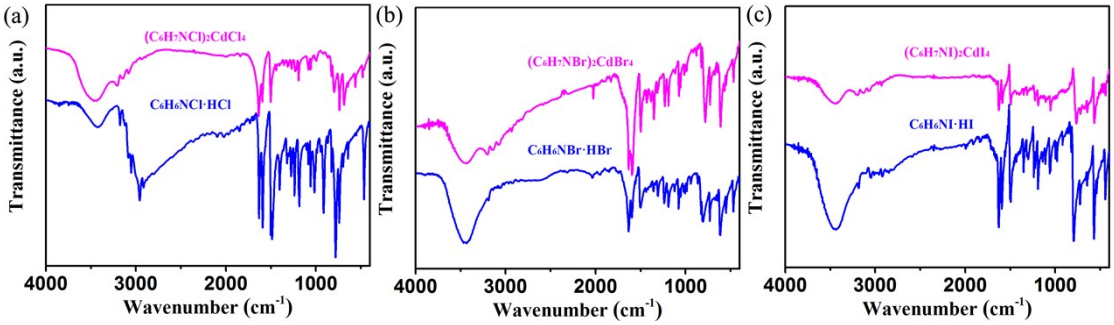

Figure S2. FT-IR spectrum of $(C_6H_7NCl)_2CdCl_4$ (a), $(C_6H_7NBr)_2CdBr_4$ (b) and $(C_6H_7NI)_2CdI_4$ (c).

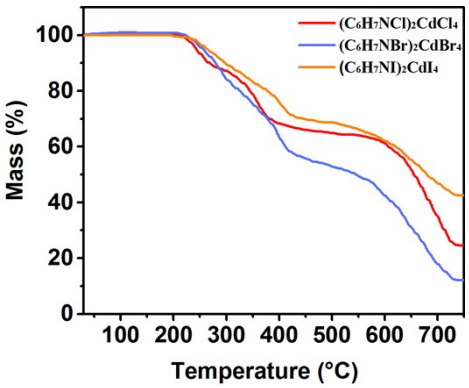

Figure S3. TGA of $(C_6H_7NCl)_2CdCl_4$, $(C_6H_7NBr)_2CdBr_4$ and $(C_6H_7NI)_2CdI_4$ (c).

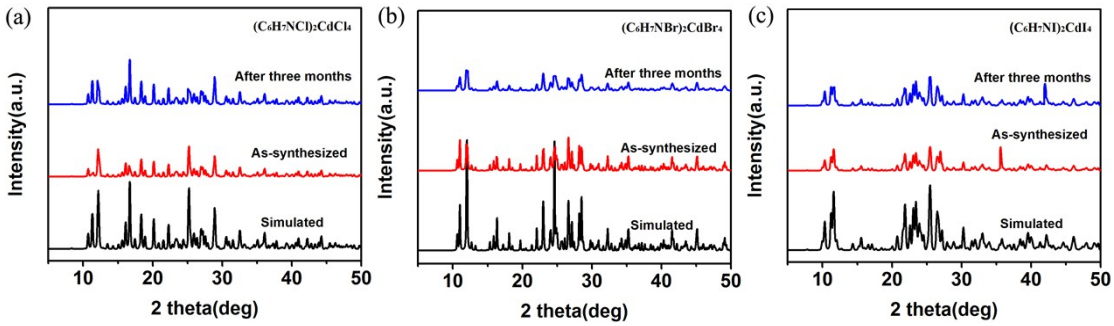

Figure S4. Experimental and simulated PXRD data of $(C_6H_7NCl)_2CdCl_4$ (a), $(C_6H_7NBr)_2CdBr_4$ (b) and $(C_6H_7NI)_2CdI_4$ (c).

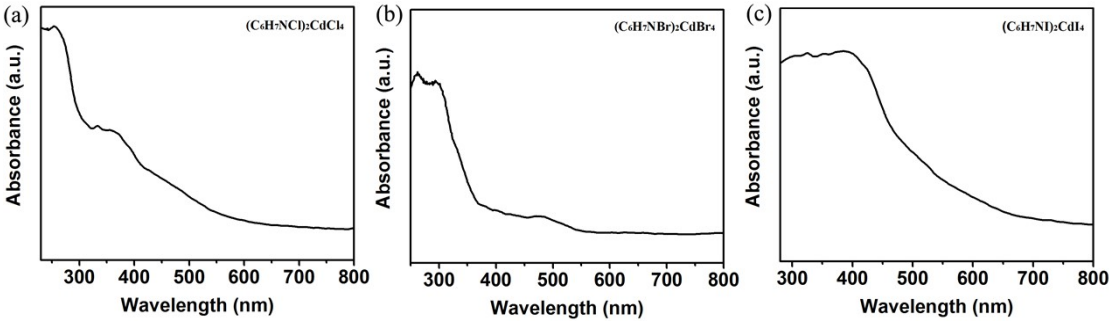

Figure S5. UV absorption spectra of $(C_6H_7NCl)_2CdCl_4$ (a), $(C_6H_7NBr)_2CdBr_4$ (b) and $(C_6H_7NI)_2CdI_4$ (c).

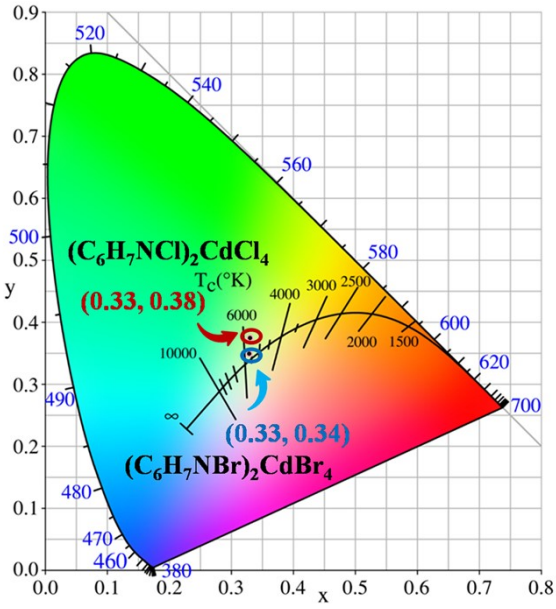

Figure S6. CIE of $(C_6H_7NCl)_2CdCl_4$ (red point) and $(C_6H_7NBr)_2CdBr_4$ (blue point).

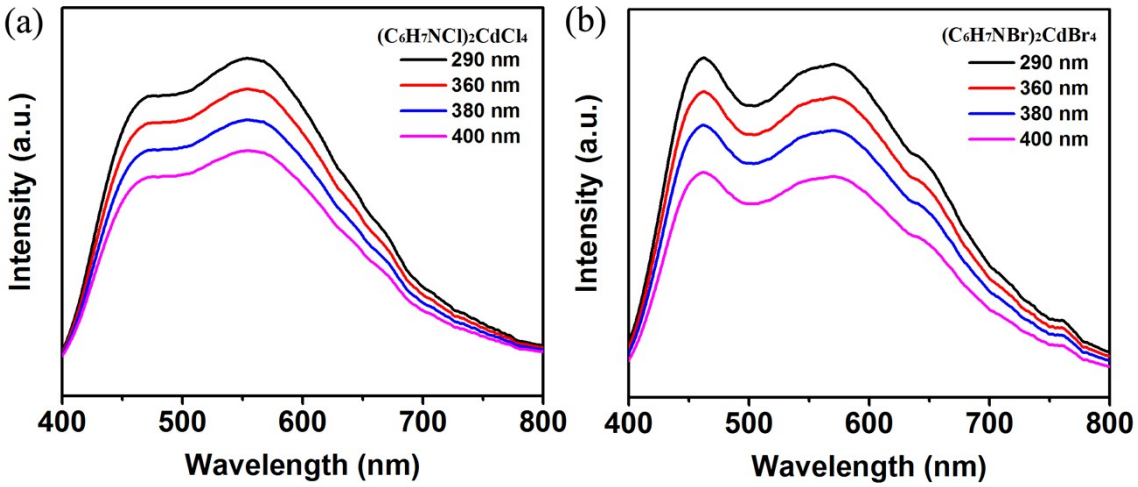

Figure S7. Emission spectra of $(C_6H_7NCl)_2CdCl_4$ and $(C_6H_7NBr)_2CdBr_4$ under different excitations.

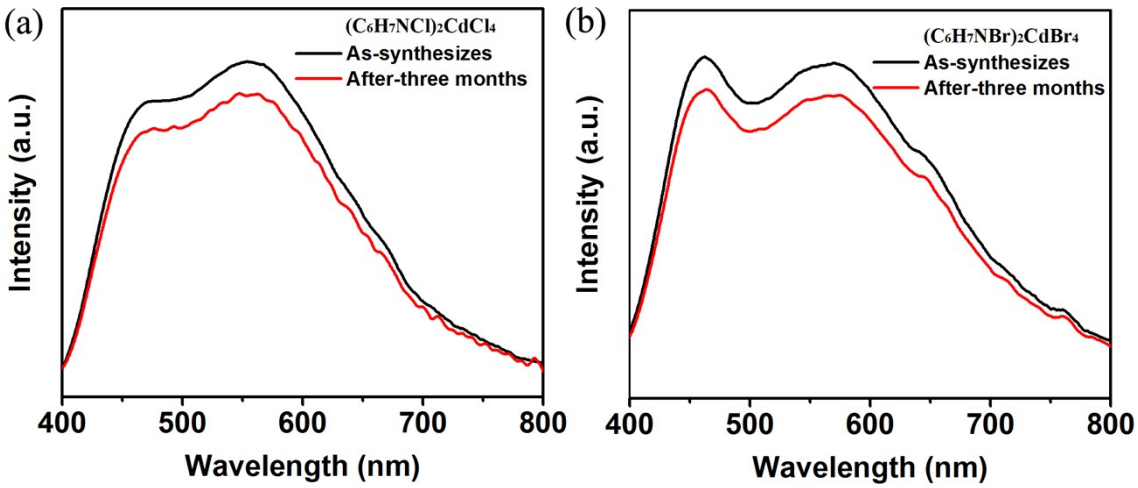

Figure S8. Emission spectra before and after three months of $(C_6H_7NCl)_2CdCl_4$ (a) and $(C_6H_7NBr)_2CdBr_4$ (b).

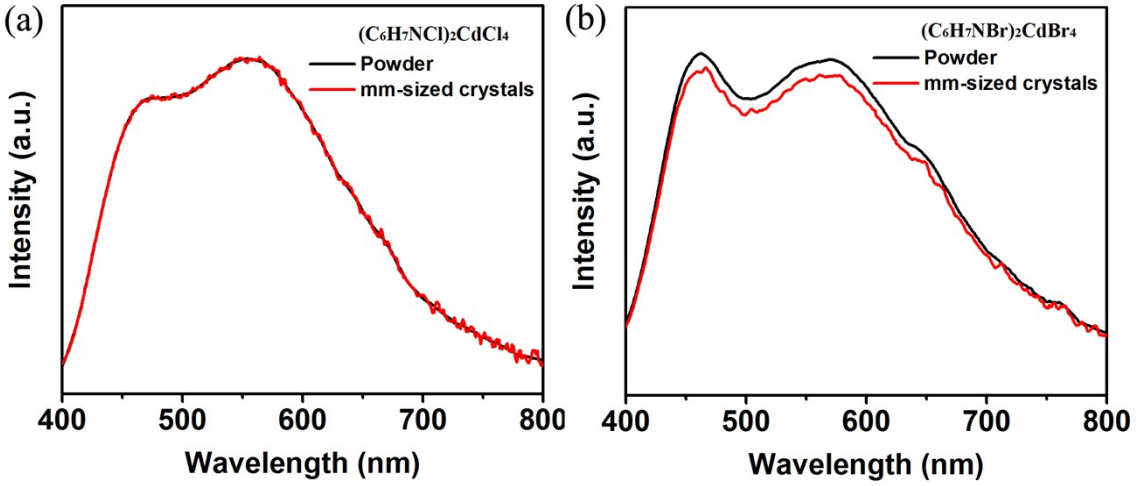

Figure S9. Emission spectra of $(C_6H_7NCl)_2CdCl_4$ (a) and $(C_6H_7NBr)_2CdBr_4$ (b) for mm-sized bulk crystals and powder sample.

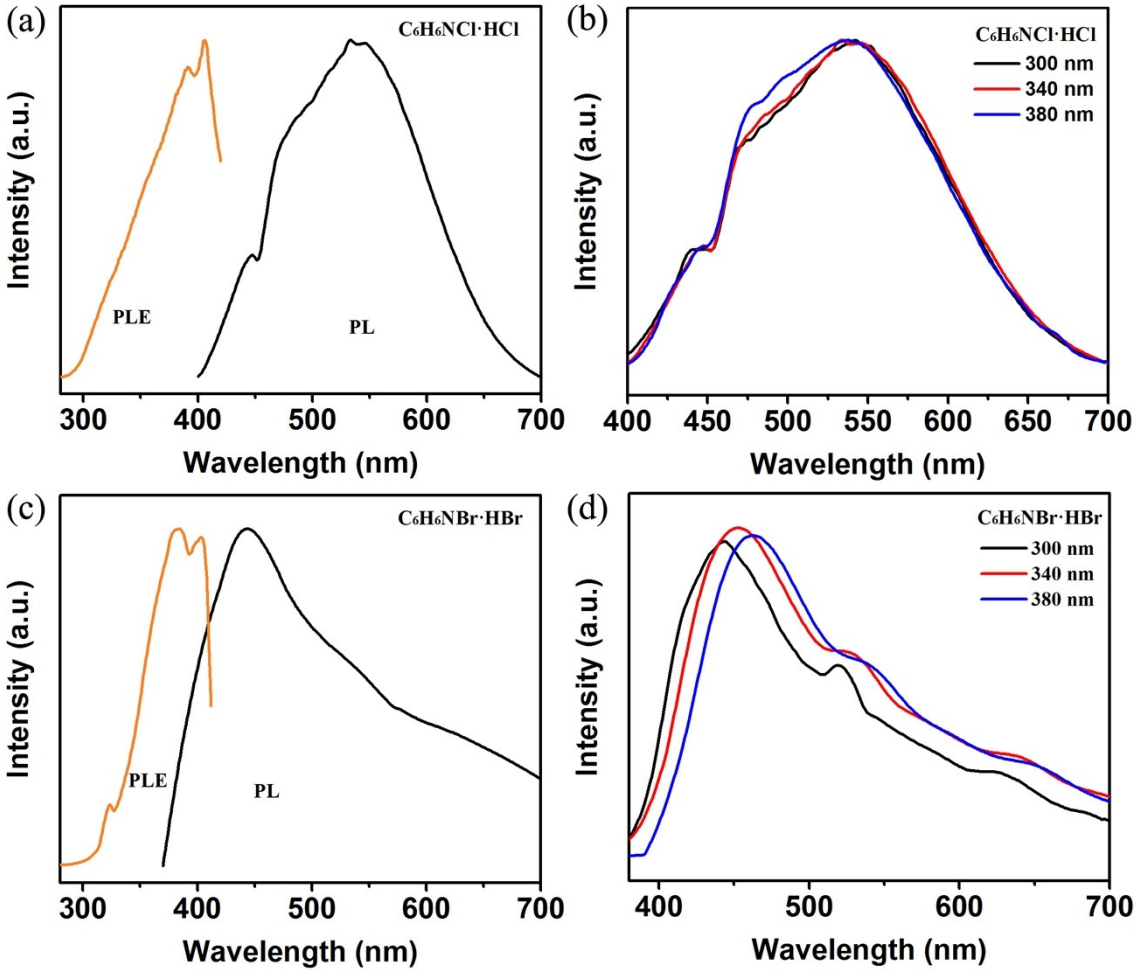

Figure S10. (a) Excitation and emission spectra of $C_6H_6NCl·HCl$, (c) $C_6H_6NBr·HBr$; (b) Emission spectra under different excitations of $C_6H_6NCl·HCl$, (d) $C_6H_6NBr·HBr$.

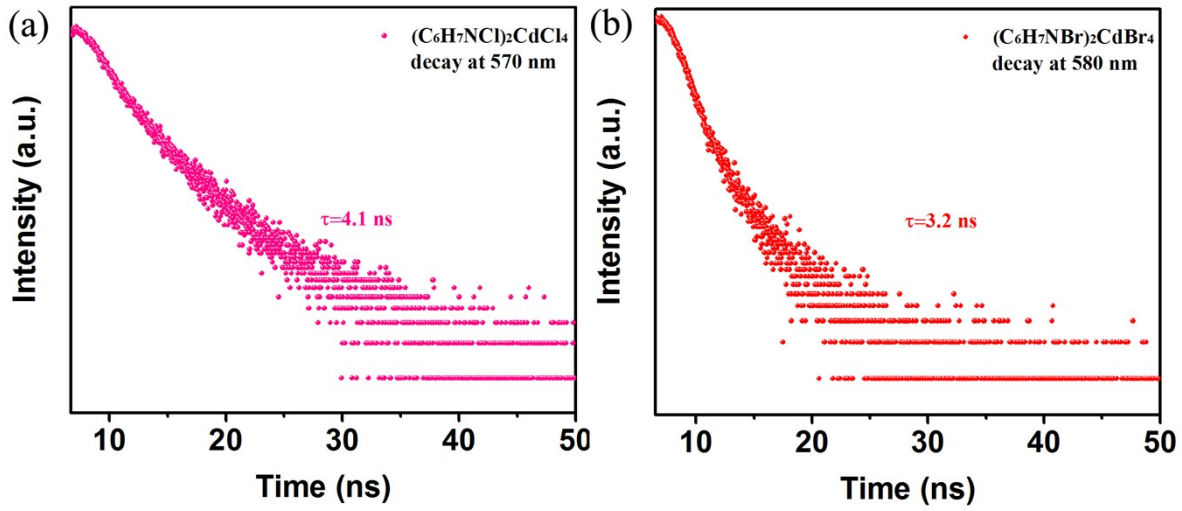

Figure S11. PL decay lifetime of $(C_6H_7NCl)_2CdCl_4$ at 570 nm (a) and $(C_6H_7NBr)_2CdBr_4$ at 580 nm (b).

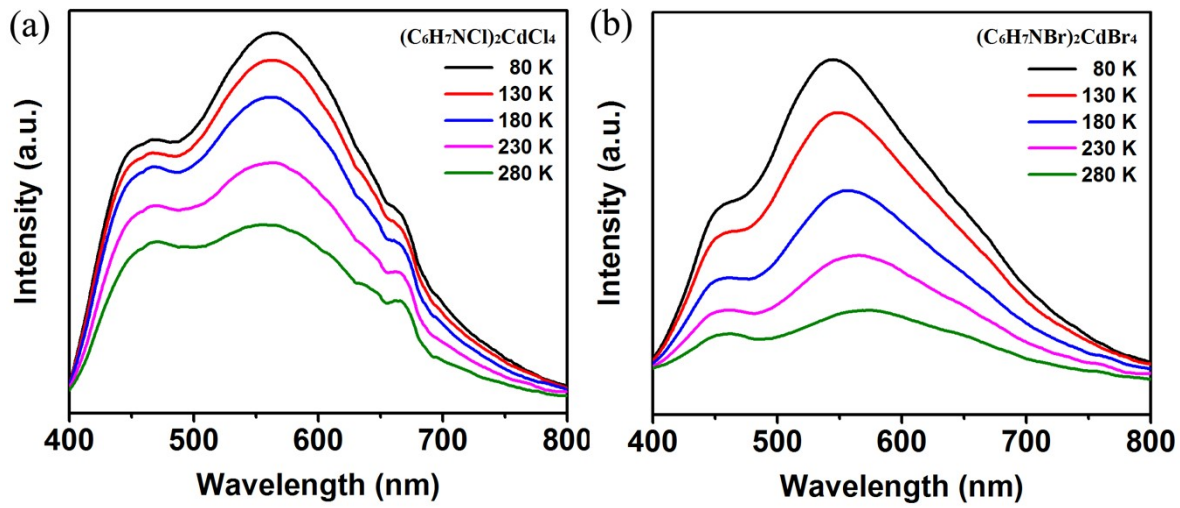

Figure S12. The temperature-dependent PL emission spectra of $(C_6H_7NCl)_2CdCl_4$ (a) and $(C_6H_7NBr)_2CdBr_4$ (b).

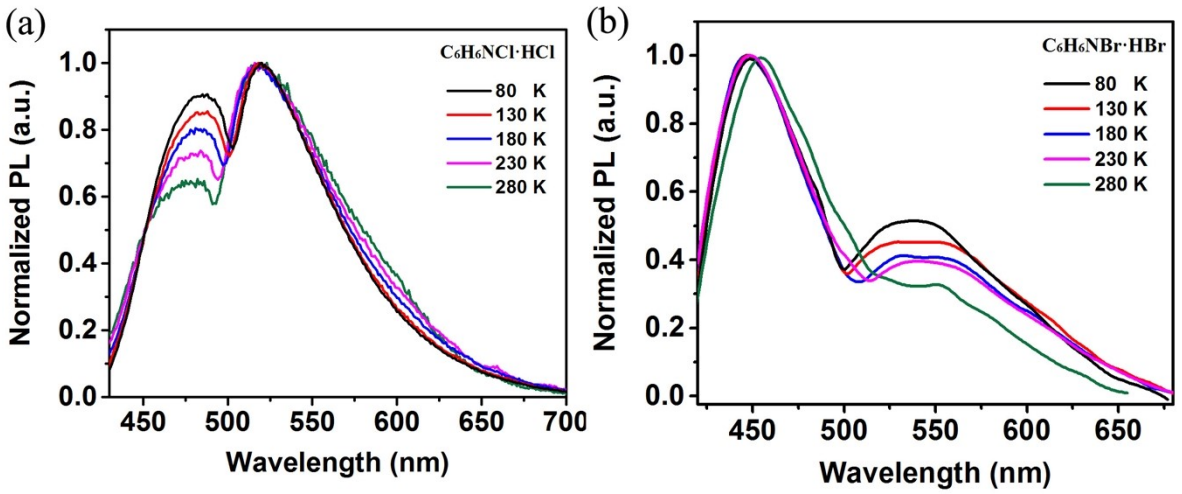

Figure S13. The temperature-dependent PL emission spectra of $C_6H_6NCl·HCl$ (a) and $C_6H_6NBr·HBr$ (b).

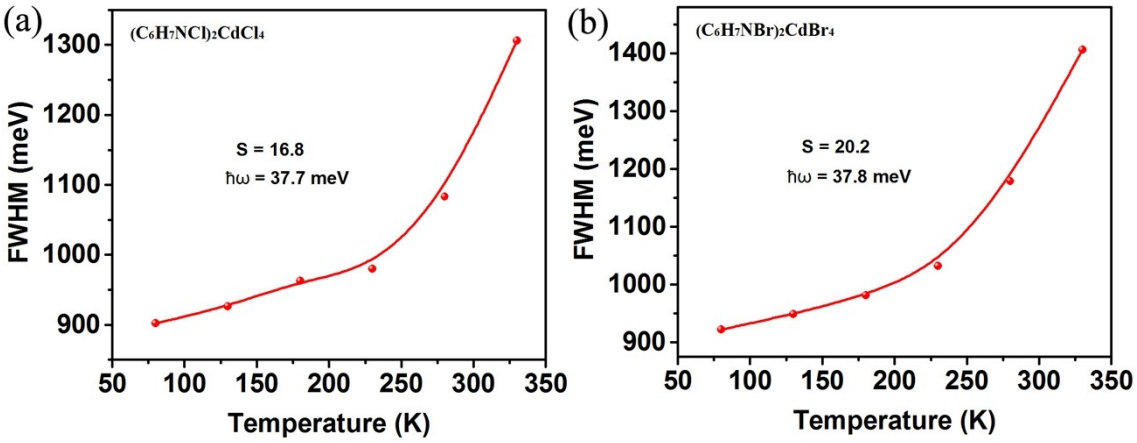

Figure S14. The temperature-dependent FWHM curve of $(C_6H_7NCl)_2CdCl_4$ (a) and $(C_6H_7NBr)_2CdBr_4$ (b).

Huang-Rhys factor (*S*) is often used to evaluate the electron-phono coupling, and the value of *S* can reflect the temperature-dependence of the electron-phono coupling. The value of *S* is a key parameter for STEs formation, and it can be obtained via the following formula:

$$FWHM = 2.36\sqrt{S}\,\hbar\omega\sqrt{coth\frac{\hbar\omega}{2k_BT}}$$

The *S* factor is calculated to be 16.8, 20.2, and $\hbar\omega$ is 37.7 meV, 37.8 meV for $(C_6H_7NCl)_2CdCl_4$ and $(C_6H_7NBr)_2CdBr_4$, respectively, indicating the strong electron-phono coupling effect and highly distorted lattice structure in $(C_6H_7NX)_2CdX_4$ to favor the formation of STEs.

Table S1. Crystal data of $(C_6H_7NCl)_2CdCl_4$, $(C_6H_7NBr)_2CdBr_4$ and $(C_6H_7NI)_2CdI_4$

Formula	$(C_6H_7NCl)_2CdCl_4$	$(C_6H_7NBr)_2CdBr_4$	$(C_6H_7NI)_2CdI_4$
Mr	511.35	778.11	1060.05
Crystal system	monoclinic	monoclinic	monoclinic
Space group	$P2_1/c$	$P2_1/c$	$P2_1/c$
Z	4	4	4
a/Å	8.3379(10)	8.55700(10)	8.9322(3)
b/Å	15.6323(10)	16.26640(10)	17.1175(9)
c/Å	14.5932(10)	14.9119(2)	15.3568(6)
α/°	90	90	90
β/°	98.3260(10)	98.1280(10)	97.486(4)
γ/°	90	90	90
V/Å ^{3}	1882.43(3)	2054.76(4)	2327.99(17)
ρ_{calc} /g cm $^{-3}$	1.804	2.515	3.025
μ/mm $^{-1}$	17.079	22.141	8. 891
F(000)	1000.0	1432.0	1864.0
R_{int}/R_{sigma}	0.0868/0.0302	0.0648/0.0201	0.0353/0.0630
Reflections	38897	47060	10866
Data/Para.	3885/198	4262/198	5282/208
R_1[a], wR_2[b][I>2σ(I)]	0.0483/0.1268	0.0363/0.0943	0.0630/0.1595
R_1[a], wR_2[b][all data]	0.0485/0.1270	0.0372/0.0949	0.0912/0.1819
$\Delta\rho_{max}$ /$\Delta\rho_{min}$/ e Å^{-3}	1.05/-1.62	1.65/-1.02	1.92/-1.36

[a] $R_1 = \Sigma||F_o| - |F_c||/\Sigma|F_o|$. [b] $wR_2 = \{\Sigma[w(F_o^2 - F_c^2)^2]/\Sigma[w(F_0^2)^2]\}^{1/2}$

Table S2. Selective bond lengths of $(C_6H_7NCl)_2CdCl_4$, $(C_6H_7NBr)_2CdBr_4$ and $(C_6H_7NI)_2CdI_4$

$(C_6H_7NCl)_2CdCl_4$		$(C_6H_7NBr)_2CdBr_4$		$(C_6H_7NI)_2CdI_4$	
Atom–Atom	Length / Å	Atom–Atom	Length / Å	Atom–Atom	Length / Å
Cd1–Cl1	2.4641(10)	Cd1–Br1	2.5763(6)	Cd1–I1	2.7862(11)
Cd1–Cl2	2.4906(10)	Cd1–Br2	2.5550(6)	Cd1–I2	2.7591(12)
Cd1–Cl3	2.4424(9)	Cd1–Br3	2.5930(6)	Cd1–I3	2.7338(11)
Cd1–Cl4	2.4272 (10)	Cd1–Br4	2.6219(6)	Cd1–I4	2.768(11)
Cl5–C12	1.770(4)	Br5-C6	1.952(5)	I6–C7	2.123(13)
Cl6–C6	1.781(4)	Br6–C12	1.933(5)	I5–C1	2.186(12)

Table S3. Selective bond angles of $(C_6H_7NCl)_2CdCl_4$, $(C_6H_7NBr)_2CdBr_4$ and $(C_6H_7NI)_2CdI_4$

$(C_6H_7NCl)_2CdCl_4$		$(C_6H_7NBr)_2CdBr_4$		$(C_6H_7NI)_2CdI_4$	
Cl2–Cd1–Cl1	100.50(3)	Br1–Cd1–Br4	106.33(2)	I1–Cd1–I2	112.04(4)
Cl4–Cd1–Cl1	112.68(4)	Br1–Cd1–Br3	112.03(2)	I3–Cd1–I4	112.66(16)
Cl4–Cd1–Cl2	111.54(4)	Br2–Cd1–Br4	110.30(2)	I2–Cd1–I4	113.10(2)
Cl3–Cd1–Cl1	112.68(4)	Br2–Cd1–Br1	112.84(2)	I3–Cd1–I1	108.42(4)
Cl3–Cd1-Cl2	105.01(3)	Br2–Cd1–Br3	113.28(2)	I2–Cd1–I1	107.89(4)
Cl3–Cd1–Cl4	113.48(3)	Br3–Cd1-Br4	101.19(2)	I4–Cd1–I1	102.00(16)